2017 American Control Conference
Sheraton Seattle Hotel
May 24–26, 2017, Seattle, USA

Trajectory Control of a Very Flexible Flying Wing

Pengyuan Qi[1], Yinan Wang[2], Xiaowei Zhao[1], Rafael Palacios[2] and Andrew Wynn[2]

Abstract— **This paper investigates the trajectory control of a very flexible flying wing model, which is derived from geometrically-nonlinear beam theory using intrinsic structural description in [1]. This model is coupled with structural dynamics, aeroelastic dynamics and flight dynamics. The control design is using a two-loop LADRC (linear active disturbance rejection control) and H^∞ scheme in both the longitudinal and lateral channels, based on a reduced-order linearised model. In each channel, the outer loop (position control) employs LADRC technique to track desired flight routes and generate attitude command to the inner loop, while the inner loop (attitude control) uses H^∞ control technique to track the attitude command generated from the outer loop and computes the control inputs to the corresponding control surfaces. The simulation tests are conducted in a reduced-order nonlinear model (the reduced-order linearised model with a quadratic nonlinear term). Simulation study shows that the trajectory control system achieves good robust and tracking performance. We mention that the simulation differences between the reduced-order and full-order nonlinear models are negligible in the case of trajectory control tests.**

I. INTRODUCTION

High Altitude Long Endurance Unmanned Aerial Vehicles (HALE UAVs) with flexible, high aspect ratio wings have seen a significant rise in commercial interest in recent years. This is in no small part thanks to a number of simulation frameworks developed to simulate the dynamics of these very flexible aircraft, which have lead to improved understanding of their unique aeroelastic behaviour. However control design for this class of air vehicles is still under-developed, where the strong coupling between structural dynamics, aeroelastic dynamics and flight dynamics has made this task much more complex and challenging than conventional aircraft.

So far, most researches focus on the aspect of aeroelastic control, including disturbance rejection and dynamic stabilisation [2], [3]. There are very limited researches on trajectory control. Shearer and Cesnik [4] studied the trajectory control of a very flexible wing-body configuration. They separated the control problem into two loops, where linear quadratic regulator (LQR) controller and dynamic inversion controller were utilized respectively in lateral and longitudinal channels to track the linear and angular velocities in the inner loop, while a nonlinear transformation together with a traditional PID controller were employed to track the commanded values of the flight path angle and roll angle in the outer loop. Simulation results showed that the control system indeed worked but the performance was limited. Raghavan and Patil [5] applied a multi-step nonlinear dynamic inversion controller coupled with nonlinear guidance law to track a pre-defined trajectory, based on the reduced order model of a high-aspect-ratio flying wing configuration. The controller was able to follow both straight line and curved gound paths successfully, however it took quite long time (approximately 400s) to eventually move to the commanded value. Dillsaver et. al. [6] investigated the trajectory control of a six-meter long flying wing using the method in [4]. But they replaced the PID controller in the longitudinal outer loop with a sliding mode controller to increase system robustness. In addition, they designed a LQG (linear quadratic Gaussian) controller with a constant pre-compensator in lateral channel to track roll and yaw angle commands. Good tracking performance taking account of gust disturbances were shown in their results, however it is well known that LQG controller can display a lack of robustness in certain cases.

In terms of modelling, the airframe of very flexible aircraft are usually modelled using beam theories to describe the aeroelastic responses associated with large structural deformations. Although nonlinear plate [7] and full 3D [8] models have also been used in this capacity, they are associated with significantly increased computational cost and not practical for control design. Different choices of state variables lead to differing beam models used in the literature, these include displacement-based models [9], strain-based models [10], mixed variational models incorporating displacement, velocity and strain [11], and intrinsic models containing velocity and strain [12]. Among them, the intrinsic structural description demonstrated the unique advantage of reducing the form of geometrical nonlinearity to second-order, leading to a nonlinear system that is easily reduced [1]. Thus this kind of reduced model is very suitable for fast simulation and control designs. Using this kind of method, a nonlinear flexible flying wing model and its nonlinear reduced-order version were developed in the same paper [1]. The aeroelastic control of this flying wing model have been investigated in [13], [14]. The present paper aims to investigate the trajectory control of this model.

Our control system is designed based on the linear model which is obtained by ignoring the nonlinear term in the reduced-order nonlinear model mentioned above, causing modelling error. Therefore it is very crucial to guarantee robustness in control designs. We propose a two-loop LADRC (linear active disturbance rejection control) and H^∞ scheme in the trajectory control system design as shown in Fig. 1, which is a novel application to very flexible aircraft. As a

[1]P. Qi and X. Zhao are with the School of Engineering, University of Warwick, Coventry CV4 7AL, United Kingdom, email: {P.Qi, Xiaowei.Zhao}@warwick.ac.uk

[2]Y. Wang, R. Palacios and A. Wynn are with the Department of Aeronautics, Imperial College London, London SW7 2AZ, United Kingdom, email: {yinan.wang09, r.palacios, a.wynn}@imperial.ac.uk

well-developed robust control technique, H^∞ method has shown big advantages in numerous areas on guaranteeing robustness. Whilst LADRC is a relatively new control technique, which is quite easy to design and has shown greater robust performance over classical PID control method. The simulation tests are conducted based on the reduced-order nonlinear model which show that our trajectory control system has good tracking and robust performances. We mention that the differences between simulations of the reduced-order and full-order nonlinear models is apparent only at very large deviations from trim equilibrium or very significant structural deformations, which are not encountered in the cases being studied in trajectory control.

II. MODELLING OF A FLYING WING

A nonlinear modal aeroelastic formulation [13] is used as a basis for creating a reduced-order aeroelastic description of the flying wing. The method uses a geometrically nonlinear structural model based on the intrinsic formulation for beams, coupled to a linear 2D aerodynamic formulation that is projected onto the structural modal basis. Furthermore a flight dynamics model with thrust, gravity and control surface effects is also included. The model reduction will be carried out via a balanced truncation of the linearised dynamics.

A. Aeroservoelastic Model

The aeroelastic formulation used in this work is described in detail in a previous publication on the subject [12]. This subsection presents key results that will form a reduced-order description of the very flexible flying wing.

Consider a flexible, high-aspect ratio airframe with control surfaces and variable engine thrust. The aircraft is modelled as a collection of geometrically nonlinear composite beams, with associated lifting surfaces that deform with the structure. Their structural dynamics are described by means of intrinsic variables everywhere on the beam reference axis s. The intrinsic variables include structural velocities (translational velocity $\mathbf{v} \in \mathbb{R}^3$ and angular velocity $\boldsymbol{\omega} \in \mathbb{R}^3$ vectors) and beam sectional forces (force $\mathbf{F} \in \mathbb{R}^3$ and moment $\mathbf{M} \in \mathbb{R}^3$ vectors) defined in the local reference frame at location s. Control surfaces are modelled by modifying the local aerodynamic lift, drag and moment coefficients of the lifting surfaces and are described by a vector $\boldsymbol{\delta}$ containing individual control surface deflection angles. Engine thrust is modelled as simple point forces and are described by a vector $\mathbf{f}_T$ containing individual engine thrust settings.

In the structural model, a Galerkin projection is used to express the intrinsic variables in terms of basis functions $\boldsymbol{\phi}_1 \in \mathbb{R}^6$ and $\boldsymbol{\phi}_2 \in \mathbb{R}^6$ as

$$\begin{aligned} \begin{pmatrix} \mathbf{v}(s,t) \\ \boldsymbol{\omega}(s,t) \end{pmatrix} &= \sum_j \boldsymbol{\phi}_{1j}(s) q_{1j}(t), \\ \begin{pmatrix} \mathbf{F}(s,t) \\ \mathbf{M}(s,t) \end{pmatrix} &= \sum_j \boldsymbol{\phi}_{2j}(s) q_{2j}(t), \end{aligned} \tag{1}$$

and the structural (elastic and rigid-body) states are defined as $\mathbf{q}_s = \begin{bmatrix} \mathbf{q}_1 & \mathbf{q}_2 \end{bmatrix}$.

In the flight dynamics model, the time-integration of the orientation (rotation matrix) $\mathbf{T} \in \mathbb{R}^{3\times3}$ and displacement vector $\mathbf{r} \in \mathbb{R}^3$ of a point is given by [15] as

$$\dot{\mathbf{T}}(s,t) = \mathbf{T}(s,t)\tilde{\boldsymbol{\omega}}(s,t), \dot{\mathbf{r}}(s,t) = \mathbf{T}(s,t)\mathbf{v}(s,t),$$

where the $\tilde{\bullet}$ symbol indicates the cross-product operator, such that for vectors $\mathbf{a} \in \mathbb{R}^3$ and $\mathbf{b} \in \mathbb{R}^3$, $\tilde{\mathbf{a}}\mathbf{b} = \mathbf{a} \times \mathbf{b}$.

The dynamics of the full aeroservoelastic system expressed by intrinsic variables described above takes the form of [12]

$$\begin{aligned} \dot{\mathbf{q}}_s =& \mathbf{A}\mathbf{q}_s + \boldsymbol{\Gamma}(\mathbf{q}_s)\mathbf{q}_s \\ &+ \left(\mathbf{H}_1(\mathbf{q}_s^*) + V_\infty \mathbf{H}_2(\mathbf{q}_a) + \mathbf{H}_{3,d}(\mathbf{q}_s)\delta_d\right)\mathbf{q}_s \\ &+ \mathbf{H}_g(\mathbf{q}_s)\mathbf{T}_0 + \mathbf{H}_T\mathbf{f}_T, && \text{(2a)} \\ \dot{\mathbf{q}}_a =& \mathbf{P}_1\mathbf{q}_s^* - V_\infty \mathbf{P}_2\mathbf{q}_a, && \text{(2b)} \\ \dot{\mathbf{T}}_0 =& \mathbf{T}_0\mathbf{N}_1(\mathbf{q}_s), && \text{(2c)} \\ \dot{\mathbf{r}}_0 =& \mathbf{T}_0\mathbf{N}_2(\mathbf{q}_s), && \text{(2d)} \end{aligned}$$

where the full set of states include structural states $\mathbf{q}_s(t)$ (a combination of $\mathbf{q}_1$ and $\mathbf{q}_2$ in (1)), additional aerodynamic states $\mathbf{q}_a(t)$ introduced to track the lift history (described below), the rigid-body orientation $\mathbf{T}_0(t)$ and displacement vector $\mathbf{r}_0(t)$ of a reference point in an inertial frame.

In equation (2a), the structural dynamic response is described by a matrix $\mathbf{A}$ and linear coupling operator $\boldsymbol{\Gamma}$, corresponding to the linear and geometrically nonlinear parts of response respectively. The influence of aerodynamic forces on the structure is described by linear operators $\mathbf{H}_1$ and $\mathbf{H}_2$, which are the instantaneous and time-dependent (lift history) aerodynamic force components on the structure respectively. An additional term $\mathbf{H}_3$ describes the aerodynamic forces caused by control surface deflections, with $\boldsymbol{\delta}_d$ being the vector containing the individual control surface deflection angles. The aerodynamic states are introduced to track the unsteady lift history of each aerofoil section along the lifting surfaces [12] as part of Theodorsen's theory. The aerodynamic coupling is also projected under the Galerkin projection (1) and cast in a modal form, resulting in the aerodynamic state equation (2b) that describes the lift history associated with each structural mode. Additionally, V_∞ used in the aerodynamic model is computed as the magnitude of the current freestream velocity at a reference point on the aircraft. The remaining external forces include the effect of thrust from the engine thrust forces $\mathbf{f}_T$ described by $\mathbf{H}_T$ matrix and the gravity acceleration described by matrix $\mathbf{H}_g$. The dynamic system (2) will be used as a basis for the subsequent model reduction and control design.

B. Model Order Reduction

The trim equilibrium is defined as the solution to (2) such that $\dot{\mathbf{q}}_s = \mathbf{0}$, $\dot{\mathbf{q}}_a = \mathbf{0}$, $\dot{\mathbf{T}}_0 = \mathbf{0}$, $\dot{\mathbf{r}}_0|_1 = 0$ and $\dot{\mathbf{r}}_0|_3 = 0$ (i.e. steady forward level flight, assuming the direction of flight is the y-axis), at which structural, aerodynamic states and the reference node orientation are $\mathbf{q}_{se}$, $\mathbf{q}_{ae}$ and $\mathbf{T}_{0e}$ respectively. We express the orientation of the reference node $\mathbf{T}_0$ by its relative rotation from the trim equilibrium orientation $\mathbf{T}_{0e}$ in terms of Euler angles (ψ_z, ψ_y, ψ_x) as $\mathbf{T}_0 = \mathbf{T}_r(\psi_z, \psi_y, \psi_x)\mathbf{T}_{0e}$ where $\mathbf{T}_r = \mathbf{I}$ at trim.

For order reduction, the system will be expanded around this trim equilibrium where we now define the new state variables as $\mathbf{q}_r = [\ (\mathbf{q}_s - \mathbf{q}_{se})^\top \quad (\mathbf{q}_a - \mathbf{q}_{ae})^\top \quad \psi_y \quad \psi_x\ ]^\top$, and the control input vector as the collection of flap and thrust actions relative to the trim level, $\mathbf{u} = [\ \Delta\boldsymbol{\delta} \quad \Delta\mathbf{f}_T\ ]$. Expanding the aeroelastic system (2) with respect to the new variable $\mathbf{q}_r$ and $\mathbf{u}$ around the trim equilibrium and retaining second-order terms produces

$$\dot{\mathbf{q}}_r = (\mathbf{S}_A + \mathbf{Q}(\mathbf{q}_r))\mathbf{q}_r + \mathbf{S}_B\mathbf{u}_c, \tag{3}$$

In the above equation, $\mathbf{Q}(\mathbf{q}_r)$ denotes the quadratic nonlinearities. The effect of the control actions through the $\mathbf{H}_{3d}$ and $\mathbf{f}_T$ terms in (2) are summarised and linearised as $\mathbf{S}_B$. Additionally, sensor measurements can be defined involving either velocities, forces and strains at different locations along the structure, as well as rotations or displacements of the body-fixed reference frame, modelled as a linear combination of the states $\mathbf{q}_r$ according to (1) and will result in the measurement matrix $\mathbf{S}_C$ and the output vector $\mathbf{y}$,

$$\mathbf{y} = \mathbf{S}_C\mathbf{q}_r. \tag{4}$$

Equations (3) and (4) form a state-space model of the flexible aircraft system with second-order nonlinearities. The model is then reduced by applying balanced truncation [16] based on the linear part of the system (the part without $\mathbf{Q}(\mathbf{q}_r)$). The resulting similarity transformation is written as

$$\mathbf{s} = \mathbf{R}\mathbf{q}_r \tag{5}$$

where the reduced state vector $\mathbf{s} \in \mathbb{R}^{N_s}$, $\mathbf{q}_r \in \mathbb{R}^{N_q}$ $\mathbf{q}_r$ with $N_s \ll N_q$, and $\mathbf{R}$ is the projection matrix from $\mathbf{q}_r$ to $\mathbf{s}$. The matrix $\mathbf{R}$ is obtained from balanced truncation process with the associated pseudo-inverse transformation $\mathbf{R}^\dagger$ where the identity $\mathbf{R}\mathbf{R}^\dagger = \mathbf{I}$ hold as a result of the reduction. Applying the transformation on full nonlinear system results in

$$\begin{pmatrix} \dot{\mathbf{s}} \\ \mathbf{y}_m \end{pmatrix} = \begin{pmatrix} \mathbf{S}_{rA} + \mathbf{Q}_r(\mathbf{s})\mathbf{s} & \mathbf{S}_{rB} \\ \mathbf{S}_{rC} & \mathbf{0} \end{pmatrix} \begin{pmatrix} \mathbf{s} \\ \mathbf{u}_c \end{pmatrix}. \tag{6}$$

For a timestep Δt, the discrete-time equivalent of the nonlinear reduced-order system (6) can be approximated as

$$\begin{pmatrix} \mathbf{s}_{i+1} \\ \mathbf{y}_m \end{pmatrix} = \begin{pmatrix} e^{(\mathbf{S}_{rA}+\mathbf{Q}_r(\mathbf{s}_i))\Delta t} & \overline{\mathbf{S}}_{rB,i} \\ \mathbf{S}_{rC} & \mathbf{0} \end{pmatrix} \begin{pmatrix} \mathbf{s}_i \\ \mathbf{u}_i \end{pmatrix}, \tag{7}$$

where $\overline{\mathbf{S}}_{rB,i} = (\mathbf{S}_{rA} + \mathbf{Q}_r(\mathbf{s}_i))^{-1}(e^{(\mathbf{S}_{rA}+\mathbf{Q}_r(\mathbf{s}_i))\Delta t} - \mathbf{I})\mathbf{S}_{rB}$ is function of $\mathbf{s}_i$. Setting the $\mathbf{Q}_r$ terms to zero results in the linearised reduced-order state-space system.

III. CONTROL DESIGN

In this section, we design the trajectory control system for the flying wing of Section II, based on its linearised reduced-order model. But the simulation tests will be based on the nonlinear model (7), which will be talked in Section IV. Since the linear model has already been decoupled, the design of the trajectory control system could be divided into two channels, the longitudinal channel and the lateral channel. As shown in the control structure in Fig. 1, a two-loop control scheme is proposed for each channel, which is explained as below.

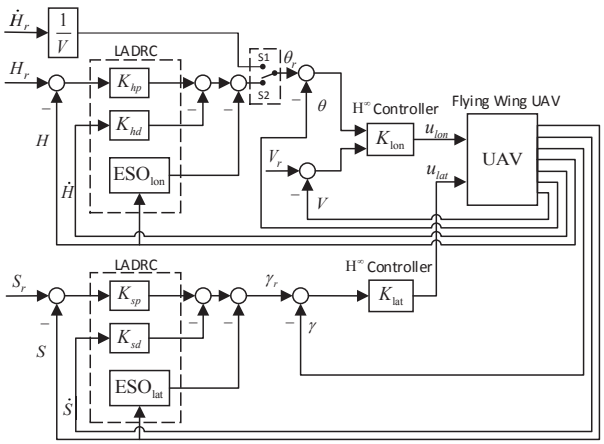

Fig. 1. Control structure of the trajectory control system. H, S, θ, V and γ denote altitude, lateral displacement, pitch angle, forward velocity and roll angle, respectively. The subscript symbol r denotes reference command, the $\dot{\bullet}$ symbol denotes time derivative, K_{lon} and K_{lat} are the H$^\infty$ controllers, $\mathrm{ESO}_{\mathrm{lon}}$ and $\mathrm{ESO}_{\mathrm{lat}}$ are the extended state observers (ESO) in LADRC, K_{*p} and K_{*d} are parameters of linear control law in LADRC.

The trim condition of the flying wing is at sea level with the speed of 12.2m/s, the specific aircraft configuration could be referred to [17]. In the longitudinal channel, both altitude and forward velocity need to be controlled. They are achieved through pitch control and velocity control respectively, by adjusting corresponding longitudinal control flaps and thrust. In this channel, to handle an altitude tracking command, the outer-loop controller is first switched to S1 "climbing control" to drive the flying wing to climb. After climbing to a close altitude, the outer-loop controller is then switched to S2 "altitude control" to activate the LADRC controller to precisely position and maintain the flying wing at the desired altitude. The climbing control generates a pitch angle command to the inner loop, which is simply equal to the climb rate command (set as $0.432m/s$, the same as the one the Helios had in its mishap flight [18]) divided by the forward velocity. The LADRC controller is designed to generate a pitch angle command for the inner loop, using altitude and vertical speed as feedback. And an inner-loop H$^\infty$ controller is designed to generate longitudinal control inputs to stabilize velocity and track the pitch angle command, using pitch angle and forward velocity as feedback.

In the lateral channel, only lateral displacement needs to be controlled, achieved through the roll control by adjusting the corresponding lateral control flaps and thrust. In this channel, an outer-loop LADRC controller is used to generate a roll angle command for the inner loop, using lateral position and lateral speed as feedback. And an inner loop H$^\infty$ controller is employed to generate control inputs with roll angle as feedback, to accomplish the lateral displacement control.

A. Inner-Loop H$^\infty$ Control Design

We now design the inner-loop H$^\infty$ controller in longitudinal channel. As described above, its role is to track the pitch angle command received from the outer loop and to maintain forward velocity simultaneously. To achieve both good tracking and robust performance, weighted H$^\infty$ synthesis method is employed, introducing weighting matrices to enhance the

disturbance rejection and parameter uncertainties attenuation performance. The control design could be seen as a standard H^∞ tracking problem, as shown in Fig. 2.

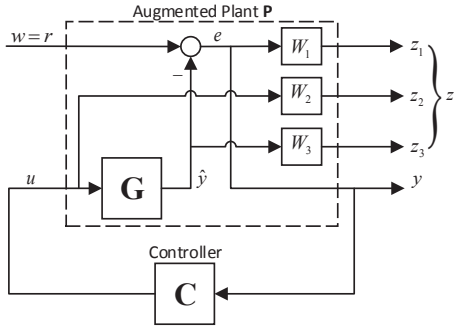

Fig. 2. Standard H^∞ tracking problem. *r*, *u*, $\hat{y}$, *e*, *z* and *y* denote reference command, control input, output of plant, error signal, weighted output and feedback signal, respectively. ***G*** and ***C*** are transfer functions of the plant and the controller.

The partitioned augmented plant **P** is comprised of the original plant **G** and the weighting matrices W_1, W_2 and W_3. The weighting matrix $W_{\rm i}(s)$ is given in the form of

$$W_i(s) = \frac{\alpha_1 s + 1}{\alpha_2 s + 1}$$

where s is the Laplace variable while α_1 and α_2 are non-zero scalers. Normally, W_1 should be selected as a low pass filter to achieve good tracking performance, W_2 should be selected as a high pass filter to achieve good robust stability against modelling uncertainties, W_3 should be selected as a high pass filter to achieve good robust stability against high frequency noise. By selecting appropriate weighting parameters and formulating the augmented plant **P**, Matlab command *hinfsyn* could be used to compute the optimal H^∞ controller in the longitudinal channel, denoted by $K_{\rm lon}$.

The design of the inner-loop H^∞ controller $K_{\rm lat}$ in the lateral channel (as shown in Fig. 1) is similar to the case in the longitudinal channel, thus it is omitted here.

B. Outer-Loop LADRC Control Design

The distinct feature of LADRC theory is estimating all the internal and external disturbances of the plant using ESO (Extended State Observer), and then taking the estimated value as compensation for the original control inputs computed by corresponding linear control law. LADRC has much less parameters to tune, compared to its nonlinear version [19]. We now design the LADRC controllers in the longitudinal and lateral channels.

1) LADRC Control Design in the Longitudinal Channel: In longitudinal channel, the altitude motion could approximately be regarded as a first-order differential equation with pitch angle θ as input and altitude H as output, i.e.

$$\dot{H} \approx -V\alpha + V\theta$$

where V is the forward velocity while α is the angle of attack, which is treated as a type of disturbance. The idea of LADRC is to construct a second order ESO with states z_{1h} and z_{2h}, where z_{1h} estimates the altitude H and z_{2h} estimates all the possible disturbances to H. With the extended state z_{2h}, the control compensator derives a compensation value u_{h*} to the control input. The actual control input u_h (pitch angle command) is equal to the computed control input u_{h0} (by linear control law) subtracted by u_{h*}. The dynamic equations of longitudinal LADRC control system are

$$\begin{cases} e_h = z_{1h} - H \\ \dot{z}_{1h} = z_{2h} - \beta_{1h} e_h + V u_h \\ \dot{z}_{2h} = -\beta_{2h} e_h \\ u_{h*} = \dfrac{z_{2h}}{V} \\ \beta_{1h} = 2\omega_h, \beta_{2h} = {\omega_h}^2 \\ u_{h0} = K_{hp} \cdot (H_r - H) + K_{hd} V_y \\ u_h = u_{h0} - u_{h*} \end{cases} \tag{8}$$

where e_h is the error between estimated altitude z_{1h} and actual altitude H. V, H_r and V_y are forward velocity, altitude command and vertical speed, respectively. β_{1h} and β_{2h} are the coefficients of longitudinal ESO defined by parameter w_h. K_{hp} and K_{hd} are the parameters of the linear control law. By tuning parameters w_h, K_{hp} and K_{hd}, good dynamic performance and good stability margin can be achieved.

2) LADRC Control Design in the Lateral Channel: In lateral channel, as shown in Fig. 3, under the assumption of small course angle and level flight, we can obtain the approximate relationship between lateral displacement S and roll angle γ as

$$\ddot{S} \approx V\dot{\psi}_k \approx \frac{L}{m}\gamma \approx g\gamma,$$

where ψ_k is the course angle, g is the acceleration of gravity.

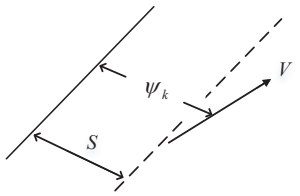

Fig. 3. Simplified model of lateral motion. S denotes lateral displacement, ψ_k denotes course angle and V denotes forward velocity. The dashed line denotes desired flight route, the solid line denotes actual flight path.

Following a similar procedure as in the case in the longitudinal channel, the dynamic equations of lateral LADRC control systems are obtained

$$\begin{cases} e_s = z_{1s} - S \\ \dot{z}_{1s} = z_{2s} - \beta_{1s} e_s \\ \dot{z}_{2s} = z_{3s} - \beta_{2s} e_s + g u_s \\ \dot{z}_{3s} = -\beta_{3s} e_s \\ u_{s*} = \dfrac{z_{3s}}{g} \\ \beta_{1s} = 3\omega_s, \beta_{2s} = 3{\omega_s}^2, \beta_{3s} = {\omega_s}^3 \\ u_{s0} = K_{sp} \cdot (S_r - S) - K_{sd}\dot{S} \\ u_s = u_{s0} - u_{s*} \end{cases} \tag{9}$$

where z_{1s}, z_{2s}, z_{3s} are the estimations of the lateral displacement, lateral speed, and all the disturbances to the lateral displacement, respectively. e_s is the error between estimated lateral displacement z_{1s} and actual lateral displacement S. g is the acceleration of gravity, S_r is the lateral displacement

command. u_{s0}, u_{s*} and u_s are the original control input computed by linear control law, the compensation value and the actual control input, respectively. β_{1s}, β_{2s} and β_{3s} are the coefficients of the lateral ESO defined by controller parameter w_s. K_{sp} and K_{sd} are the parameters of the linear control law. By tuning parameters w_s, K_{sp} and K_{sd}, good dynamic performance and good stability margin of the LADRC controller can be achieved.

IV. STABILITY ANALYSIS AND SIMULATION RESULTS

Following the design procedure in Section III, the inner-loop H^∞ controllers and the outer-loop LADRC controllers in both channels are obtained. This section demonstrates the performance of this trajectory control system by stability analysis and simulations. Recall from the Introduction section that the simulation differences between the full-order nonlinear model (2) and the reduced-order nonlinear model (7) are negligible in the case of trajectory control tests.

A. Stability Margins

Recall that the most important objective of the control design in this paper is to guarantee system robustness. Through Bode diagram analysis, we could obtain the magnitude and phase margins of the altitude control system are 28.4 dB and 90.1° respectively, while the ones of the lateral displacement control system are 15.5 dB and 66.4° respectively. These stability margin figures show good robustness has been achieved against modelling uncertainties and external disturbances.

B. Step Response

To illustrate the dynamic tracking performance of the designed controllers, simulations are conducted under the linear model and nonlinear model (7) respectively. The simulation time step is set to Δt= $0.05s$. Step responses of the altitude control systems and the lateral displacement control systems are shown in Fig. 4 and Fig. 5, respectively.

Fig. 4 shows the rising time of the 10-meter step response of the altitude control system is approximately 46 seconds and it has no steady error. The nonlinear term in the nonlinear model (7) barely has any impact on the altitude tracking response compared to the response under linear model. The nonlinear term shows a bit impact on stabilizing of the forward velocity, where the largest amplitude change is only 0.2m/s and the velocity is stabilized quickly in both linear and nonlinear models. All the four control inputs are in reasonable regions. All these demonstrate good tracking and robust performances of the altitude control system. As reflected in Fig. 5, similar good tracking performance and good robustness have been obtained by the lateral displacement control system.

C. Gust Wind Response

This subsection demonstrates the control performance against disturbance, taking altitude control as an example. The simulation test is conducted based on the nonlinear model (7) with a wind gust applied in the vertical direction

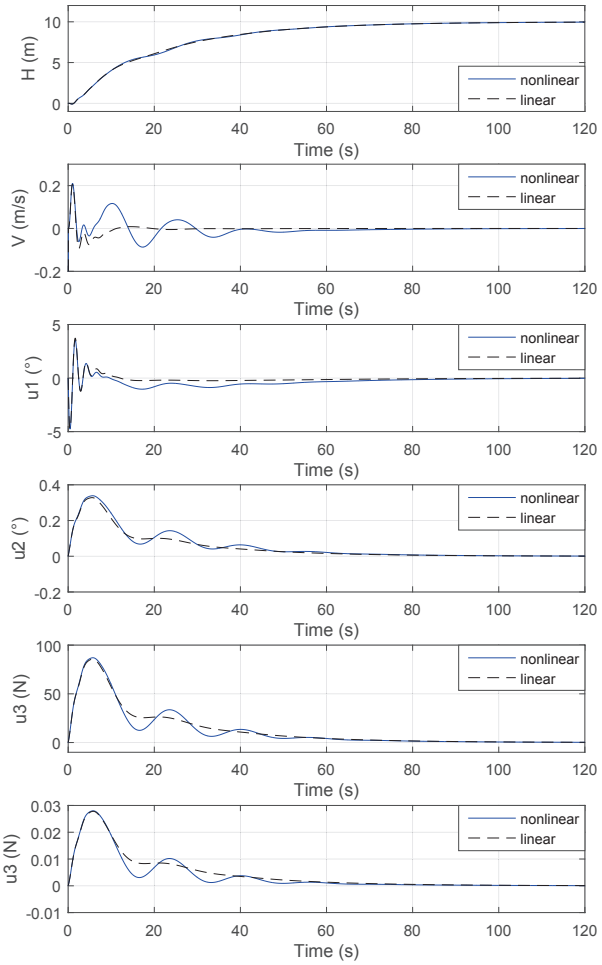

Fig. 4. Step response of altitude control. H, V denote altitude and forward velocity, u1, u2, u3, u4 are control action of simultaneous flap, control action of symmetric differential flap, control action of simultaneous thrust and control action of symmetric differential thrust respectively, as defined in [14]. Note that all the simulation results are deviations from trim conditions.

during the time period between 20s and 30s, where the aircraft is flying at the altitude of 200m. Fig. 6 shows the advantages of LADRC (the solid line) over PID control (the dotted line). It is clear to see that both controllers can drive the aircraft back to 200m eventually. However the LADRC controller has much smaller overshoot and faster converge rate than the PID controller. Note that to make reasonable comparison, the PID controller had been tuned to have similar step response performance as the LADRC controller before conducting simulation tests under wind gust.

D. Trajectory Tracking Performance

This subsection illustrates the trajectory tracking performance of the designed trajectory control system. Five way points A to E are defined by actual geographic positions (in longitude, latitude and altitude), forming the desired flight route. We design a guidance algorithm to guide the flying wing to track this desired route. The actual flight route compared with the desired one is shown in Fig. 7. It is clear that the flying wing is able to track well the desired position commands, thus good tracking performance has been achieved.

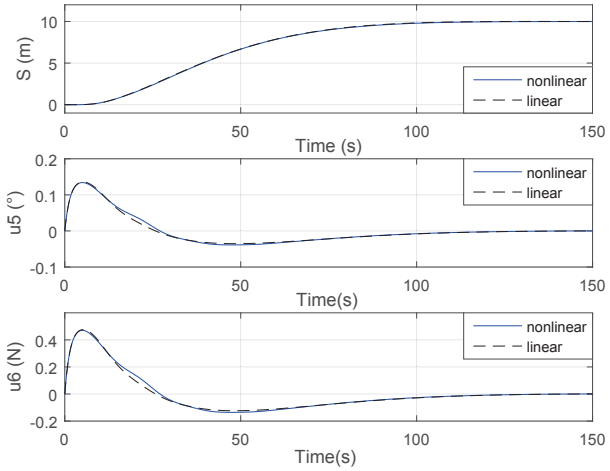

Fig. 5. Step response of lateral displacement control. S denotes lateral displacement, u5 and u6 denote control action of antisymmetric differential flap and control action of antisymmetric differential thrust respectively. Note that all the simulation results are deviations from trim conditions.

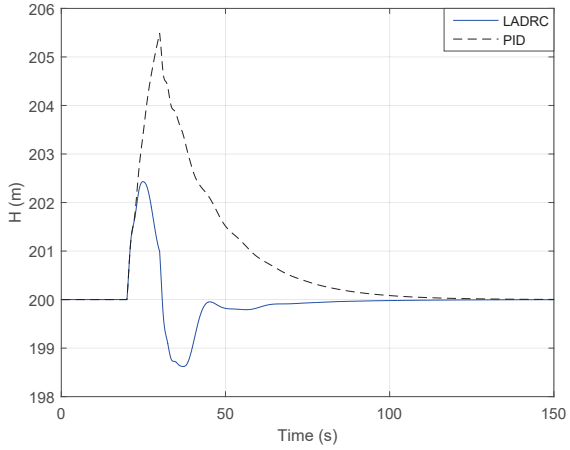

Fig. 6. Altitude responses of a flying wing with two different types of controller (LADRC vs PID) in the longitudinal outer loop in Fig. 1. H denotes altitude. The magnitude of the applied vertical gust is 1m/s with the duration of 10s. It is with classical (1-cos) model.

V. CONCLUSIONS

A two loop control scheme based on LADRC and H^{∞} control technique for the trajectory control of a very flexible flying wing has been proposed. Simulations have shown that the trajectory control system has good tracking and robust performances.

REFERENCES

[1] Y. Wang, W. Andrew, and R. Palacios, "Model-predictive control of flexible aircraft using nonlinear reduced-order models," in *57th AIAA/ASCE/AHS/ASC Structures, Structural Dynamics, and Materials Conferencde*, 2016.

[2] M. J. Patil, D. H. Hodges, and C. E. S. Cesnik, "Nonlinear aeroelasticity and flight dynamics of high-altitude long-endurance aircraft," *Journal of Aircraft*, vol. 38, no. 1, pp. 88–94, 2001.

[3] C. M. Shearer and C. E. Cesnik, "Nonlinear flight dynamics of very flexible aircraft," *J. of Aircraft*, vol. 44, no. 5, pp. 1528–1545, 2007.

[4] C. M. Shearer and C. E. S. Cesnik, "Trajectory control for very flexible aircraft," *Journal of Guidance, Control, and Dynamics*, vol. 31, no. 2, pp. 340–357, 2008.

[5] B. Raghavan and M. J. Patil, "Flight control for flexible, high-aspect-ratio flying wings," *Journal of guidance, control, and dynamics*, vol. 33, no. 1, pp. 64–74, 2010.

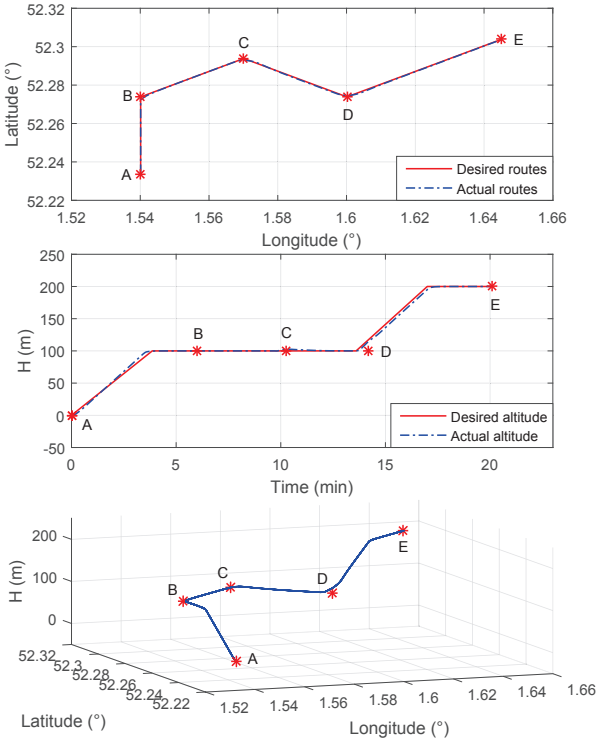

Fig. 7. Trajectory tracking performance. The red solid line from A to E shows the desired flight route defined by actual geographic positions and altitudes, the blue dot-dashed line shows the actual flight route. The red asterisks in the first and third sub-figures denote the scheduled way points.

[6] M. J. Dillsaver, C. E. Cesnik, and I. V. Kolmanovsky, "Trajectory control of very flexible aircraft with gust disturbance," in *AIAA Atmospheric Flight Mechanics (AFM) Conference*, 2013, p. 4745.

[7] D. Tang, H. Yamamoto, and E. Dowell, "Flutter and limit cycle oscillations of two-dimensional panels in three-dimensional axial flow," *Journal of Fluids and Structures*, vol. 17, no. 2, pp. 225–242, 2003.

[8] L. Demasi and E. Livne, "Dynamic aeroelasticity of structurally nonlinear configurations using linear modally reduced aerodynamic generalized forces," *AIAA Journal*, vol. 47, no. 1, pp. 70–90, 2009.

[9] R. J. Simpson and R. Palacios, "Numerical aspects of nonlinear flexible aircraft flight dynamics modeling," in *54th AIAA Structures, Structural Dynamics, and Materials Conference, Boston, USA*, 2013.

[10] W. Su and C. E. S. Cesnik, "Dynamic response of highly flexible flying wings," *AIAA Journal*, vol. 49, no. 2, pp. 324–339, 2011.

[11] M. J. Patil, D. H. Hodges, and C. E. Cesnik, "Limit-cycle oscillations in high-aspect-ratio wings," *Journal of fluids and structures*, vol. 15, no. 1, pp. 107–132, 2001.

[12] Y. Wang, A. Wynn, and R. Palacios, "Nonlinear modal aeroservoelastic analysis framework for flexible aircraft," *AIAA Journal*, vol. 54, 2016.

[13] Y. Wang, W. Andrew, and R. Palicios, "Nonlinear model reduction for aeroelastic control of flexible aircraft described by large finite-element models," in *Proceedings of the AIAA/ASMe/ASCE/AHS/SC Structures, Structural Dynamics, and Materials Conference*, 2014.

[14] Y. Wang, "Aeroelastic modelling and control of very flexible air vehicles using a nonlinear modal formulation," Ph.D. dissertation, Department of Aeronautics, Imperial College, London, 2015.

[15] Y. Wang, R. Palacios, and A. Wynn, "A method for normal-mode-based model reduction in nonlinear dynamics of slender structures," *Computers & Structures*, vol. 159, pp. 26–40, 2015.

[16] H. Kwakernaak and R. Sivan, *Linear optimal control systems*. Wiley-interscience New York, 1972, vol. 1.

[17] M. J. Patil and D. H. Hodges, "Flight dynamics of highly flexible flying wings," *Journal of Aircraft*, vol. 43, no. 6, pp. 1790–1799, 2006.

[18] T. E. Noll, J. M. Brown, and M. E. Perez-Davis, "Investigation of the helios prototype aircraft mishap report," *Tech. rep*, NASA, 2004.

[19] Z. Gao, "Scaling and bandwidth-parameterization based controller tuning," in *Proceedings of the American control conference*, vol. 6, 2006, pp. 4989–4996.